INVESTIGATION OF LIGHT OIL DEPRESSURISATION WITH A DYNAMIC NETWORK MODEL: A STUDY OF RELATIVE PERMEABILITIES

I. Bondino, S. R. McDougall, Heriot-Watt University and G. Hamon, Total

This paper was prepared for presentation at the International Symposium of the Society of Core Analysts held in Toronto, Canada, 21-25 August 2005

ABSTRACT

Hydrocarbon recovery involving reservoir depressurisation is a topic of great interest in the petroleum community at present. However, one of the main problems that reservoir engineers face is the acquisition of reliable data related to relative permeability for input into conventional reservoir simulators. Unfortunately, results from macroscopic core depletion experiments are not easily interpreted, as there is often great uncertainty regarding the physical mechanisms taking place in the core — indeed, the experiments themselves are fraught with difficulties and virtually impossible to undertake at field depletion rates. A clearer understanding of the associated physical phenomena would consequently be highly desirable.

In this paper, a pore scale depressurisation network simulator previously used to model heavy oil primary depletion (SCA 2003-11), has been substantially extended in order to focus on the behaviour of very light oils. On the basis of the specific chemical and physical characteristics of such systems (low oil viscosity, high oil formation volume factors and in the present case, very low interfacial tensions), a dynamic network model is presented that takes into account the principal physical processes occurring during pressure depletion of light oils, including gravitational migration, viscous effects and oil shrinkage. In this context, the effect of the high oil shrinkage factors, gravitational and viscous forces on the nucleation, and growth and movement of bubbles is studied for the final prediction of the associated gas-oil relative permeabilities.

A number of important findings have emerged from this work. For example, we find that light oil depressurisation is the result of a complex interaction of gravitational forces, capillary effects, oil shrinkage factors and, contrary to expectation, viscous forces. In particular, it is seen that viscous biased bubble growth and viscous mobilization of gas ganglia can predominate at certain times during laboratory depletion experiments. The network simulator is also used to model primary and tertiary experimental depletions. The implications on oil production of the underlying physical processes and the corresponding relative permeabilities are discussed with reference to the current literature.

INTRODUCTION

The main objective of a depressurisation core experiment is to estimate hydrocarbon production under reservoir conditions and — usually via history-matching procedures — to infer associated relative permeabilities and critical gas saturations for use in field studies. However, depressurisation experiments are difficult to undertake at typical reservoir depletion rates and laboratory data must be carefully interpreted before extrapolation to field rates can be undertaken in a meaningful way. Whilst a unique interpretation of the underlying physical processes governing such experiments would be highly desirable, this is difficult to achieve without recourse to some sort of modelling framework. Indeed, the literature pertaining to depressurisation studies has highlighted some of the difficulties involved, with different researchers employing a diverse range of experimental techniques using differing intrinsic rock and fluid properties (for example, consider the wide range of values for critical gas saturation reported in [1,2,3], from 0.5% to 27%). In general, we find that depressurisation experiments seldom fit into a predetermined and predictable hierarchy: generalizations are extremely elusive and each experiment should be interpreted on a case by case basis.

In recent years, it has been possible to conduct theoretical studies of depressurisation using pore-scale network simulators [4,5,6,7,8]. Although these works enabled to investigate the Sgc dependence on a series of parameters, they often involved too simplistic definitions of critical gas saturation (such as the formation of sample-spanning gas clusters), which might not be representative of the near-wellbore regions where gas bubbles can flow even if non connected [9, 10]. More recently [11] the first steps have been taken towards practical applications of depressurisation network models to core-scale experiments by directly history-matching production data from heavy oil depletion experiments. These developments are seen as a crucial step towards consistent interpretation of core-scale depressurisation experiments. Conventional reservoir simulators are unable to incorporate many of the physical processes governing solution gas drive (such as non-equilibrium effects, discontinuous gas flow and rate-dependent bubble densities), and a process-specific pore-scale simulator acquires special value as an important interpretative tool.

In the work presented in this paper, a set of sensitivities is proposed to describe the combined effect of oil shrinkage and gravitational forces in light oil depletion; furthermore it is seen that viscous forces can be important for volatile critical fluids causing the mobilization and break-up of gas bubbles. In addition, the network model is used to model experimental data for both primary and tertiary depletion and to derive the associated critical gas saturations and relative permeabilities.

THE DYNAMIC NETWORK MODEL

The drainage mechanisms associated with the development of the non-wetting gas phase during pressure depletion is examined by means of a pore scale simulator originally developed by McDougall and Mackay [6] and McDougall and Sorbie [7]. In this work, the underlying modelling formulation has been significantly expanded on the basis of

new theoretical and experimental observations. Although issues such as progressive nucleation were already included in [8] and [11], important additional phenomena, such as oil shrinkage and viscous mobilization of bubbles, have been included here. A generalized model of pore shapes/volumes and conductivities has also been introduced but will not be discussed further here (for details see [12]). The shrinkage and mobilization features will be presented below.

A model for viscous mobilization of gas bubbles

In the presence of strong pressure gradients, bubble growth can become biased along the direction of the prevailing pressure gradient; furthermore bubbles can be mobilized and break-up. This is accounted for in the simulator by perturbing capillary entry pressures in order to account for the local variations in fluid pressure and recording the interim positions of all advancing meniscii (see [13]). In particular, a net capillary entry pressure is associated with every pore:

$$P^{NET} = \frac{2\sigma_{og}\cos\theta}{r} - \Delta P^{VIS} \qquad (1)$$

where σ_{og} is the gas oil interfacial tension, θ the gas-oil contact angle, r is the capillary entry radius and ΔP^{VIS} is the viscous pressure gradient across the pore.

At high pump withdrawal rates (i.e. fast depletion), the net capillary entry pressure P^{NET} for gas to invade a given oil-filled neighbour can differ significantly from that given by Laplace's law. A growth bias in the direction of the viscous pressure field is the net result. In some cases, P^{NET} can even become negative and gas is then able to migrate spontaneously as the viscous forces become bigger than the capillary threshold. Once a gas cluster becomes mobilized, bubble break-up events become possible (although total gas volume is conserved). This phenomenon is modelled here by considering the snap-off of migrating gas structures by oil, leading to bubble fragmentation. The model realistically reproduces bubble mobilisation under the effect of large viscous pressure gradients and also accounts for gas fragmentation.

Interface Tracking During Mobilization

In the modelling of viscous flow, when $P^{NET}<0$, bubbles become mobilized and the movement of gas-oil interfaces during this period needs to be tracked. This is achieved by first considering all interface movement throughout the network model and calculating the time required for the first oil-filled pore to be fully displaced by gas. All menisci positions are subsequently updated, the pressure field is recalculated and the process repeated until either all migration has ceased or the next depletion step has occurred.

Note that the filling time of a pore (and therefore the movement of the interface) is a function of both the capillary entry radius and the pore body radius. The latter is

distributed throughout the network prior to depletion in a manner that is consistent with both a previously-reported anchoring procedure [14] and experimental poro-perm data.

Oil Shrinkage Model

PVT relationships and gas transfer through the liquid phase into the bubbles define the process of gas growth during depressurisation. In critical fluids this can be accompanied by significant oil shrinkage, as dissolved gas leaves the oleic phase. An algorithm has been included that reduces the size of an oil cluster according to its loss of dissolved gas mass. The volume of oil that needs to be shrunk is calculated from PVT relationships (namely the oil formation volume factor, Bo). This means that oil shrinkage is perfectly accounted for in any situation where equilibrium has been achieved. In the new algorithm, once dissolved gas has transferred to the free gas phase through diffusion, thereby increasing the size of the bubble, further gas expansion is possible into the pores spaces vacated by the retiring oil. Stochastically, a higher probability of shrinking exists in those oil pores that are close to large gas clusters because of the larger gas-oil interface available for diffusion. Hence, oil pores close to large gas clusters are more likely to be shrunk.

SENSITIVITIES USING ANCHORED NETWORKS

The pore network model with the extensions described above is used to analyse the depressurisation of a volatile oil (see Table 1): this is a critical fluid and so, just below bubble point, the gas saturation increases very rapidly. The controlling thermodynamic input parameters required to simulate the depressurisation experiments are: 1) the interfacial tensions; 2) the densities of oil, gas and water; 3) the diffusivities of gas (in oil, in water); 4) the volume of dissolved gas in the oil, at equilibrium, at reservoir conditions (GOR); 5) the oil formation volume factors, Bo and 6) the oil and gas viscosities. The pressure-dependencies of these parameters have been approximated by polynomial functions up to saturation pressure on the basis of reported experimental data for the fluid.

The networks were also anchored to specific core samples. The methodology used is described elsewhere [14]. The adopted pores size distribution is a truncated normal distribution:

$$f(r) = N(R\max - r)(r - R\min)\exp\left[-\frac{(r-\bar{r})^2}{2\sigma^2}\right] \qquad \text{Rmin} < r < \text{Rmax}$$

In this study two different permeability set-ups have been adopted, one of low permeability (K=4.99mD, ϕ=15.49%) and one of a high permeability (K=300mD, ϕ=23%). The anchoring procedure described in [14], was performed and the results can be resumed as follows:

(Rmin=0.6E-6m, Rmax=7.0E-6m, pore connectivity (Z)=5, L=61.4E-6m) Low K
(Rmin=5.0E-6, Rmax=36.0E-6, pore connectivity (Z)=6, L=145.0E-6) High K

Experimental porosity and permeability were also matched.

Sensitivity to Oil Shrinkage and Gravity

A number of sensitivities have been performed to evaluate the role of gravitational effects at the pore-scale for the two permeability set-ups above. Figure 1 shows 2-D network models of dimensions 80X80 pores,where 1 bubble has been instantaneously nucleated at P=Pb (depletion rate 58 psi/day). The buoyancy effects are evaluated by comparing the real situation (on the left for each pair of figures) with one where buoyancy is artificially turned off. For the less permeable set-up we see from cases (a) and (b) that the bubble is slightly buoyant only during the very early stages of the depletion, at Pb-P=155psi; the situation stabilizes very quickly because the gas-oil interfacial tension rapidly increases during the depressurisation. For the highly permeable core, cases (c) and (d) show that buoyancy is important and more sustained. From Figure 1 it is also possible to see how gas develops rather quickly due to the critical properties of the fluid. Gas not only grows by mass transfer of light components from the oil and expansion but also re-fills pore spaces from which the oil has shrunk (according to the oil volume factor). In Figure 2 we again make use of the potential offered by the simulator, whereby different factors can be isolated and evaluated singularly. Here the oil is no longer allowed to shrink and we see that the bubble has grown to a far lesser extent at a given pressure (compare for example Figure 1b and Figure 2a for the less permeable core or Figure 1d and Figure 2b for the highly permeable one). What is perhaps most important is that the impact of gravitational forces changes accordingly: at the same pressure no buoyancy effect is observed for the less permeable case simply because the bubble has not grown to the critical size which would allow buoyancy to play an important role. Conversely, for the highly permeable case, a gas cap forms quickly. These examples show clearly that very light oil depressurisation is the result of a complex interaction of gravitational forces, capillary effects and oil shrinkage factors.

Sensitivity to Viscous Effects

The effect of viscous forces upon volatile oil depletion is now considered. An experiment using the same fluid and low permeability rock material described above (K=4.99 mD) was undertaken at a depletion rate of 58psi/day. The experiment was found to exhibit an average pressure gradient of dP/dl=212 psi/meter. This experimental value was tested in the simulator for a qualitative investigation of the effect of viscous forces during the depletion. Figure 3 shows the dynamics of depletion in a 2-D 80X40 network at different pressure intervals (the direction of the pressure gradient is towards the top). The pre-existing gas clusters in Figure 3a are mobilized and broken up (Figure 3b) and a flow of dispersed gas bubbles in oil soon occurs. The situation stabilizes at lower pressures (Figure 3e), when capillary forces become too high for further mobilization to take place. This is because interfacial tension is continuously increasing during depletion (Figure 4a). Figure 4b reports the number of viscous mobilization events during the simulation. For each of these events a bubble has been mobilized and moved into another pore along the direction of the viscous pressure gradient; oil re-imbibition takes place simultaneously. It can be seen that viscous mobilization is present only during the very early stages of the depressurisation process and more specifically in the pressure interval 5100psi<P<Psat (where the gas oil interfacial tension is still very low). The gas relative

permeabilities corresponding to this process are reported in Figure 5. Here, unsteady-state relative permeabilities for dispersed gas flow are shown together with quasi-steady state relative permeabilities for free gas flow. For the former (viscous dominated) the gas flow of disconnected gas bubbles out of the network is measured and the relative permeability calculated according to:

$$K_{rg} = \frac{\mu_g q_g}{KA} \frac{L}{\Delta P_o} \tag{2}$$

where the pressure gradient in oil is used instead of that in gas (cf. Javadpour and Pooladi-Darvish [15]). At lower pressure, gas bubble mobilization stops and the unsteady-state relative permeability consequently becomes zero. Conversely, free gas flow emerges at around this time and can be described by a quasi-steady state relative permeability (Krg becomes non-zero at the formation of a sample-spanning gas cluster). Both dispersed gas flow and free, connected gas flow appear to be characteristic of light oil depletion experiments under these conditions. Note that the critical gas saturation for unsteady-state gas flow is lower (Sgc^{us}=2.5% when $Krg^{us}\neq 0$) than the steady state one at the formation of a spanning gas cluster (Sgc^{ss}=9.5% when $Krg^{ss}\neq 0$).

PREDICTION OF EXPERIMENTAL PRODUCTION DATA

The network model has also been used for the prediction of experimental production data from a light oil depletion experiment. In this case, the fluid used in the experiments was again fluid 1 (Table 1); a core with the same low permeability characteristics described above was used (K=4.99 mD). The depletion rate was again 58 psi/day

By using a network of dimensions 15X15X15 sandwiched between two buffer networks (in order to reproduce larger systems), an excellent prediction of the experimental values was achieved (Figure 6a). A progressive nucleation algorithm was used as described in [8] and [11] with a Rayleigh distribution of cavity sizes in the range [$5X10^{-8}$ m, $10X10^{-8}$ m] which eventually nucleated a bubble density of 1 bubble every 233 pores. Bubbles effectively nucleated instantaneously due to the very low gas-oil interfacial tension. The system was seen to approach equilibrium very quickly, even at the relatively high laboratory depletion rate of 58 psi/day. This is due to the fact that the bubble density was sufficiently high to guarantee fast equilibration. The critical free gas saturation from the network model (defined as the saturation at which a spanning cluster formed) was found to be Sgc=18.1%. The corresponding relative permeability curve is shown in Figure 6b.

The network model has also been used for the prediction of a tertiary depletion experiment (Swi=70%) in order to assess the dynamics of oil displacement in a water-flooded reservoir. In this case, the experimental curves exhibit a great deal of complexity — at around P=1000psi a rapid increase in water saturation is visible probably due to heterogeneity effects and/or capillary end effects. The 3-phase network simulator predicts the behaviour quite well up to this point (Figure 7a), although gas saturation is slightly

underestimated during the early stages. Figure 7b shows a prediction of the 3-phase steady-state relative permeabilities: oil is disconnected throughout all the simulation and so steady-state *Kro*=0 at every pressure. Oil would not be produced as a continuous phase, only as discontinuous slugs.

The tertiary Krg curve is also superimposed in Figure 6b for a direct comparison with the primary depletion curve: the two curves do not show substantial differences. In particular the tertiary Krg is not as suppressed as found in [10] but more in agreement with the results in [16]. This clearly points out to the different methodologies proposed in the literature for the determination of Krg (different history matching procedures for example) but could also depend on other effects such as the presence of viscous forces as the wellbore is approached. As shown in Figure 5b the unsteady state gas relative permeability can become very low as the interfacial tension increases (when gas becomes less easily mobilized by viscous forces): in this sense the exact structure of the Krg curve clearly depends on the particular fluid properties and distance from the well.

It is interesting to note that the critical gas saturation for the tertiary depletion is lower than that found in the primary case, contrary to popular expectation (see [3]), but in agreement with more recent observations [17]. In fact we have Sgc=14.3% (compared to 18.1% from primary depletion), although it should be noted that gas becomes connected very late in the tertiary depletion, at Pb-P=1682psi (after 29 days). In primary depletion gas was connected at Pb-P=600 psi (after 10.3 days). The presence of large quantities of water consistently decreases the dissolved gas available and bubble growth is much slower. This explains the retarded appearance of the sample-spanning gas cluster.

Discussion of Critical Gas Saturations and Sample Size

The question of whether tertiary depletion is characterised by higher critical gas saturations would actually depend upon the particular dynamics of gas growth. For example, the wettability properties of the sample can play a role, as can the scale at which the experiment or simulation is carried out. Moreover, the impact of gravitational forces at different lengthscales and different wettability conditions could be an important consideration when interpreting laboratory data.

In fact, it turns out that the network model can be used to shed some light on this matter by upscaling networks and observing the subsequent evolution behaviour. This can be achieved by increasing the pore volumes (and lengths) to reproduce the true core dimensions: now a single element notionally represents some *region* of pore-space characterized by an equivalent capillary entry radius. Visual investigations in 2D networks become quite helpful at this point and are shown in Figure 8 for both virgin and waterflooded cases. In the virgin case, the bubble elongates because of gravity and reaches the top of the system quite early in the depletion with Sgc=26.6% at Pb-P=812psi (Figure 8c). In the water-flooded case, the bubble slowly grows in place and reaches the top of the system much later (Figure 8d). The water-flooded case at the same depletion pressure (case c, Pb-P=812psi) shows far less gas present, with no discernible elongation

of the bubble: water is constraining the bubble growth. Eventually, at Pb-P=4234 psi, the gas bubble reaches the top of the network at Sgc= 43.5% (note that the critical gas saturations presented here relate to 2D network models and can only be compared qualitatively with the low values presented earlier for 3D models). In these simple 2D simulations (with water-oil contact angle 0^o), the presence of water prevents bubbles from elongating, they reach the outlet quite late in the depletion, and Sgc is higher than that seen in the virgin case. Under different wettability conditions, however — water-oil contact angle 40^o, say — we could expect the tertiary Sgc to be *lower* than that found in the virgin depletion, as capillary forces would be comparatively weaker in this case and gravitational bias would increase. This is also in agreement with recent experimental observations [17].

CONCLUSIONS

A 3-phase depressurisation simulator has been presented that incorporates oil shrinkage and gas mobilization phenomena under conditions of high pressure gradients.

The depressurisation of a critical fluid has been followed under two different permeability scenarios: a high degree of oil shrinkage has been seen to characterize the growth of the gas phase, with gravitational effects being almost negligible at the pore scale for the less permeable sample. We have also shown how buoyancy effects are mitigated in critical fluid depressurisation experiments even in *high* permeability material — this is due to isotropic oil-shrinkage dominating the evolution process.

It has been shown that viscous effects can cause gas bubble mobilization and break-up, especially at high fluid pressures, where capillary barriers are more easily overcome by viscous forces (as gas oil interfacial tension is very low at this stage). It is seen that, if viscous forces are present, a light oil depletion experiment can be described by two relative permeabilities — one unsteady-state (for dispersed gas flow), and another steady state (for continuous gas flow).

Furthermore experimental production data were successfully modelled for both primary and tertiary depletion and the corresponding relative permeabilities were presented. The predicted relative permeabilities agree with the most recent data in the literature. Supersaturations were monitored throughout the simulations and the primary depletion systems were found to remain close to equilibrium even at a depletion rate of 58 psi/day. This was due to the instantaneous nucleation of a considerable number of bubbles. This implies that the laboratory data should also be applicable at reservoir depletion rates.

For tertiary depletion, a lower critical gas saturation was found (although Sgc occurred at a much lower pressure). We conclude that the general tenet that tertiary depletion is characterised by higher critical gas saturations can often be misleading — the configuration of evolving gas clusters actually depends upon a wide range of interacting factors, including oil shrinkage, buoyancy effects, and the underlying connectivity of the aqueous and oleic phases (the relative importance of each being strongly affected by core

wettability). Hence, such broad conclusions are too simplistic and should be treated with caution.

ACKNOWLEDGEMENTS
The authors would like to thank Total for financial and technical assistance throughout the course of this study.

REFERENCES
1. Moulu, J., C. and Longeron, D.: "Solution-gas drive: experiments and simulation", Proc., 5th European Symposium on improved oil recovery, 1989.
2. Firoozabadi, A., Ottesen, B. and Mikklesen,M.: "Measurement of supersaturation and critical gas saturation", SPE Form. Eval., 337-344, 1992.
3. Kortekaas, T., F., M. and Poelgest, F., V.: "Liberation of solution gas during pressure depletion of virgin and watered-out oil reservoirs", SPE 19693, 1989.
4. Li, X. and Yortsos, Y.C.: "Critical gas saturation: modeling and sensitivity studies. SPE 26662, 1993.
5. Hawes, R., I., Dawe, R., A. and Evans, R., N.: "Theoretical model for the depressurization of waterflooded reservoirs". Trans. IchemE, Vol. 74, Part A, 1996.
6. McDougall, S.R. and Mackay, E.J.: "The impact of pressure-dependent interfacial tension and buoyancy forces upon pressure depletion in virgin hydrocarbon reservoirs. Trans IchemE 76 (A), 553-561, 1998.
7. McDougall, S.R., Sorbie, K.S.: "Estimation of critical gas saturation during pressure depletion in virgin and waterflooded reservoirs". Petr. Geosc. 5, 229-233, 1999.
8. Bondino, I., McDougall, S. R., and Hamon, G.: "Pore Network Modelling of Heavy Oil Depressurisation: a Parametric Study of Factors Affecting Critical Gas Saturation and 3-Phase Relative Permeabilities", SPE 78976, 2002.
9. Egermann, P. and Vizika, O.: "A new method to determine critical gas saturation and relative permeability during depressurization in the near-wellbore region", SCA2000-36, presented at the 2000 SCA Symposium, Abu Dhabi.
10. Egermann, P., Banini, S. and Vizika, O.: "Depressurization under tertiary conditions in the near-wellbore region: experiments, visualization and radial flow simulations", SCA2003-15, presented at the 2003 SCA Symposium, Pau, France.
11. Bondino, I., McDougall, S.R. and Hamon G.: "Interpretation of a long-core heavy oil depletion experiment using pore network modelling techniques", SCA 2003-11, presented at the 2003 SCA Symposium, Pau, France.
12. Bondino, I.: "The application of pore-scale modelling techniques to pressure depletion in porous media", PhD Thesis, Institute of Petroleum Engineering, Heriot-Watt University, Edinburgh, U.K.
13. McDougall, S.R., Salino, P.A. and Sorbie, K.S.: "The effect of interfacial tension upon gas-oil relative permeability measurements: interpretation using pore-scale models", SPE 38920, 1997.
14. McDougall, S., R., Cruickshank, J. and Sorbie, K., S.: "Anchoring methodologies for pore-scale network models: application to relative permeability and capillary pressure prediction", SCA 2001-15, presented at the 2001 SCA Symposium, Edinburgh, U.K.
15. Javadpour, F. and Pooladi-Darvish, M.: "Network modelling of apparent-relative permeability of gas in heavy oils", J. Can. Petr.Tech., 43 (4), pp. 23-30, April 2004.

16. Goodfield, M. and Goodyear, S.G.: "Relative permeabilities for post-waterflood depressurization", SPE 83958, 2003.
17. Petersen, Jr, E.B., Agaev, G.S., Palatnik, B., Ringen, J.K., Øren, P.E. and Vatne, K.O.: "Determination of critical gas saturation and relative permeabilities relevant to the depressurization of the Statfjord Field", SCA 2004-33, presented at the 2004 SCA Symposium, Abu Dhabi.

Table 1. Fluid properties

P_{sat} (saturation pressure)	5537 psia
G/O IFT @ P=5235 psia	0.03 mN/m
W/O IFT @ P=5221 psia	33.5 mN/m
G/W IFT @ P=5221 psia	35.2 mN/m
Gas density at P=5400 psia	420 kg/m3
Oil density at P=5400 psia	507 kg/m3
D_G in oil @ 5069 psia	$3*10^{-5}$ m^2/day
GOR @ P=5537psia	656.4 sm3/sm3
Bo @ P=5537psia	3.03
Oil Viscosity @ P=5537psia T=121°C	0.12 cPo

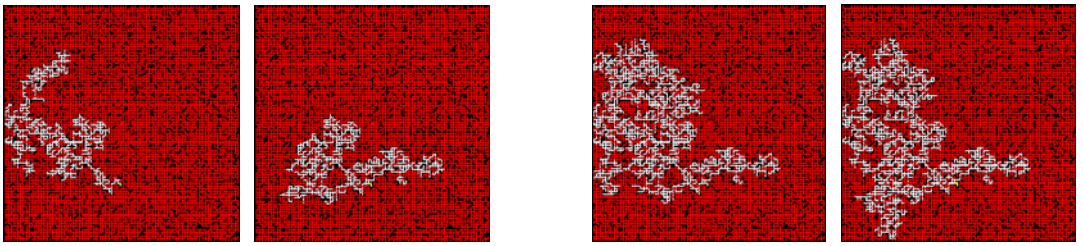

Low K (a) Pb-P=155psi (b) Pb-P=406 psi

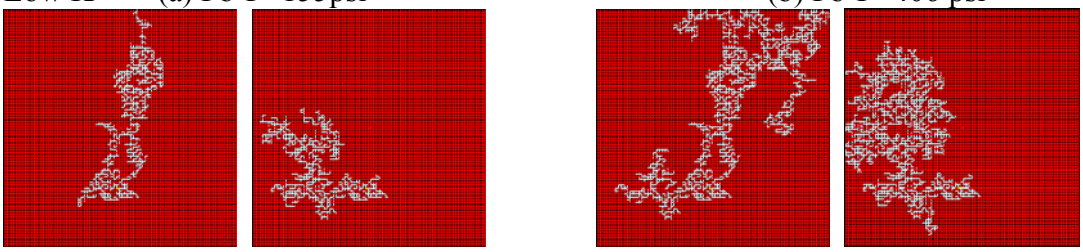

High K (c) Pb-P=155psi (d) Pb-P=406 psi

Figure 1. Buoyancy effects, network model of dimensions 80X80. For each pair of figures, buoyancy is included on the left

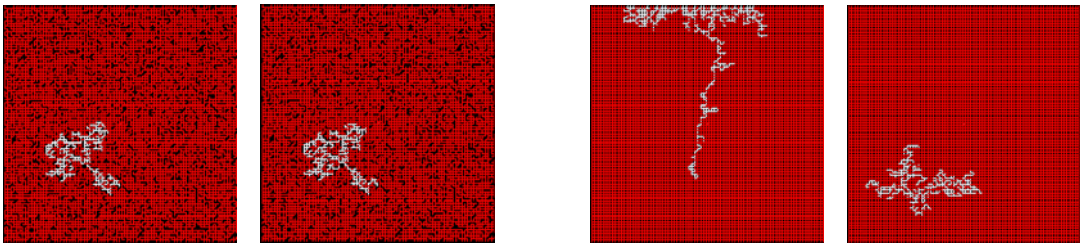

(a) Low K, Pb-P=406 psi (b) High K, Pb-P=406 psi

Figure 2. Shrinkage turned off. For each pair of figures, buoyancy is included on the left

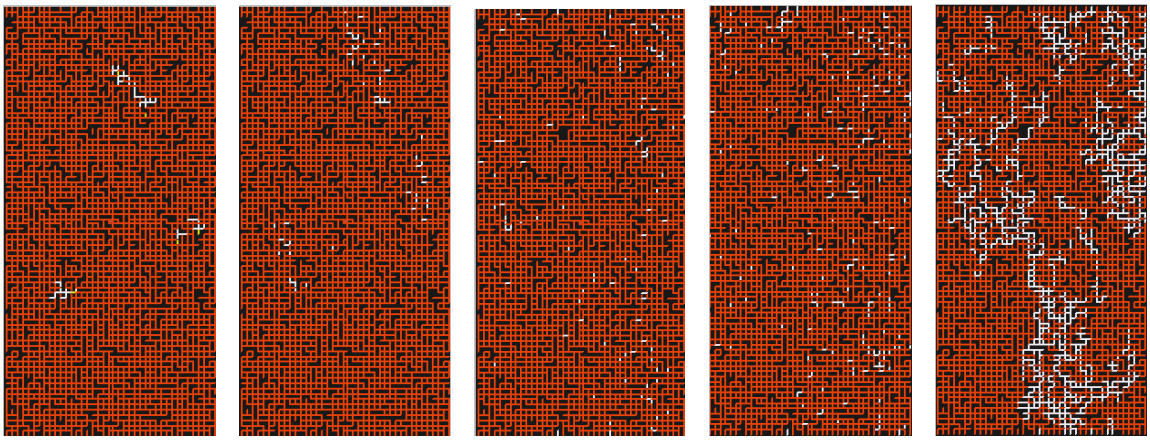

(a) (b) (c) (d) (e)

Figure 3. Depletion of volatile oil at dp/dt=58psi/day, dP/dl=212 psi/meter in a 80X40 network. (a) Pb-P=19psi prior to migration, (b) Pb-P at 19psi post migration, (c) Pb-P=39psi, (d) Pb-P=77psi, (e) Pb-P=522 psi

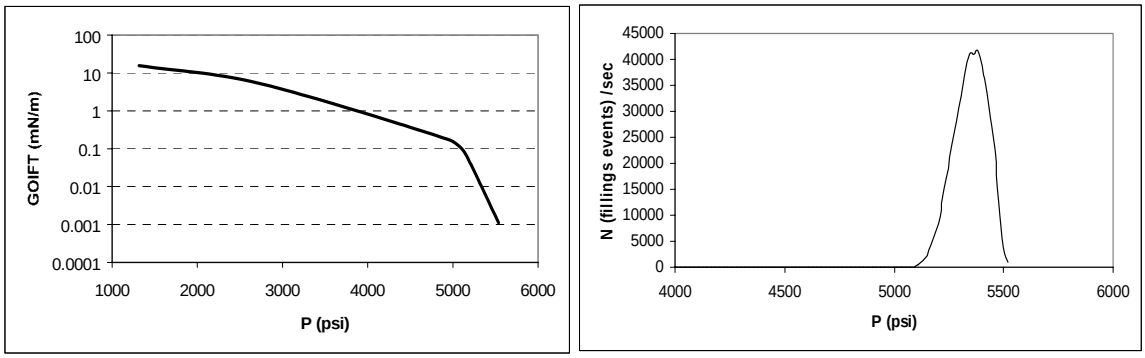

(a) (b)

Figure 4. Gas-oil interfacial tension Vs pressure (a) and number of viscous mobilization events (b)

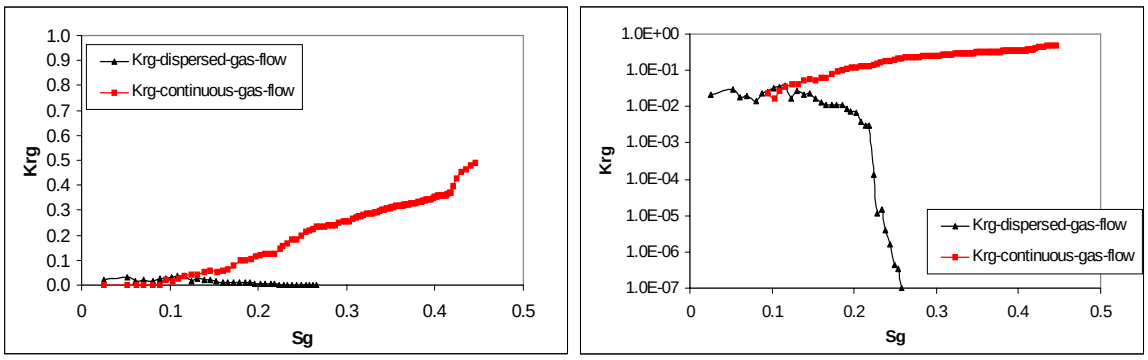

(a) (b)

Figure 5. Gas relative permeabilities measured in a simulation with viscous forces in a 15X15X15 network (dP/dl=212 psi/meter, dP/dt=58 psi/day); (b) semi-log representation

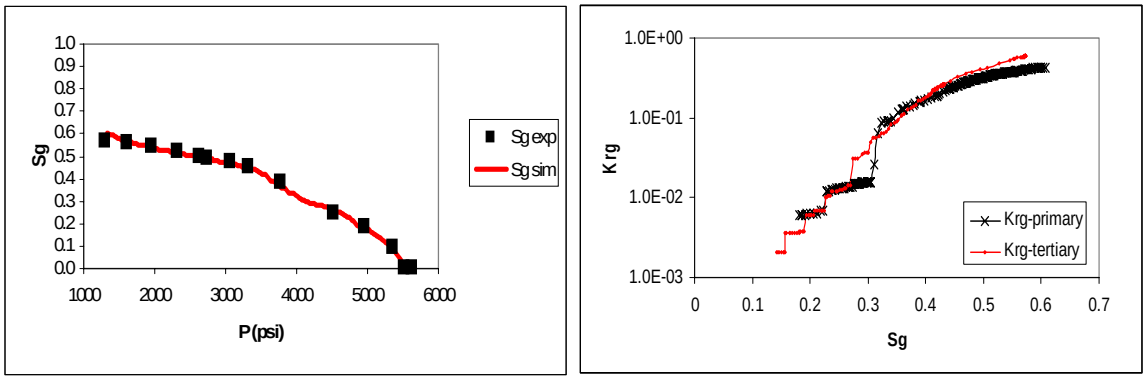

(a) (b)

Figure 6. (a) Prediction of experimental gas saturation for primary depletion. (b) Corresponding gas relative permeabilities from network modelling

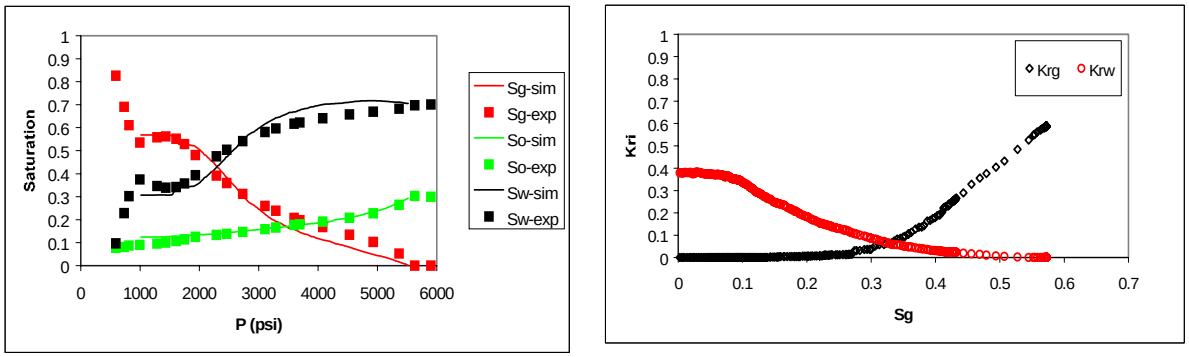

(a) (b)

Figure 7. Prediction of experimental data for tertiary depletion (a) and associated Kri curves (b) (Krg for tertiary is also shown in Figure 6b for comparison with primary)

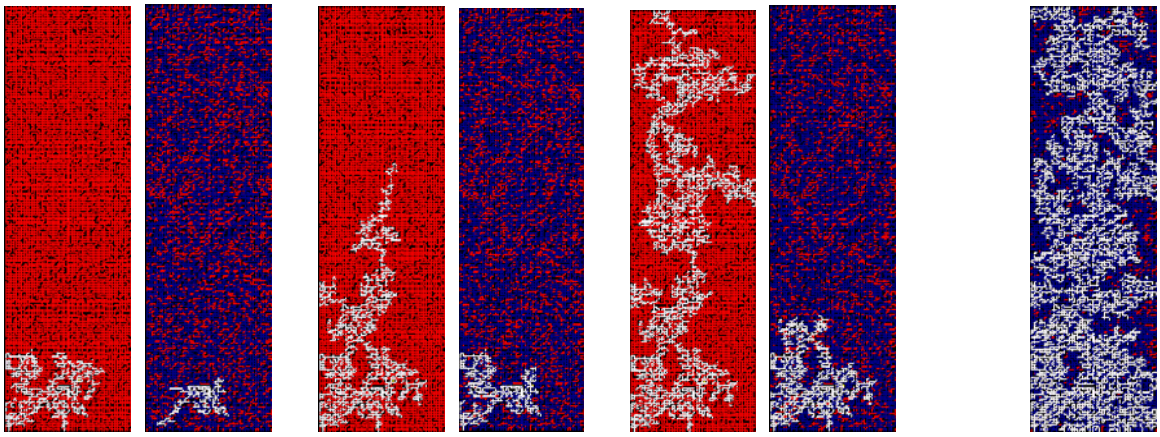

V (a) WF V (b) WF V (c) WF (d) WF

Figure 8. Gas evolution in a virgin (V) and a waterflooded (WF) system (Swi=70%). (a) Pb-P=174psi; (b) Pb-P=348 psi; (c) Pb-P=812 psi; (d) Pb-P=4234 psi. In the virgin system Sgc=26.6%; in the waterflooded system Sgc=43.5%